Nat. Hazards Earth Syst. Sci., 17, 1285–1303, 2017
https://doi.org/10.5194/nhess-17-1285-2017

Natural Hazards and Earth System Sciences
Open Access
EGU

Application of Landsat-8 and ALOS-2 data for structural and landslide hazard mapping in Kelantan, Malaysia

Amin Beiranvand Pour and Mazlan Hashim

Geoscience and Digital Earth Centre (INSTeG), Universiti Teknologi Malaysia, Johor Bahru, UTM Skudai, 81310, Malaysia

Correspondence to: Amin Beiranvand Pour (beiranvand.amin80@gmail.com, a.beiranvand@utm.my) and Mazlan Hashim (mazlanhashim@utm.my)

Received: 28 May 2016 – Discussion started: 4 July 2016
Revised: 18 December 2016 – Accepted: 4 July 2017 – Published: 28 July 2017

Abstract. Identification of high potential risk and susceptible zones for natural hazards of geological origin is one of the most important applications of advanced remote sensing technology. Yearly, several landslides occur during heavy monsoon rainfall in Kelantan River basin, Peninsular Malaysia. Flooding and subsequent landslide occurrences generated significant damage to livestock, agricultural produce, homes and businesses in the Kelantan River basin. In this study, remote sensing data from the recently launched Landsat-8 and Phased Array type L-band Synthetic Aperture Radar-2 (PALSAR-2) on board the Advanced Land Observing Satellite-2 (ALOS-2) were used to map geologic structural and topographical features in the Kelantan River basin for identification of high potential risk and susceptible zones for landslides and flooding areas. The data were processed for a comprehensive analysis of major geological structures and detailed characterizations of lineaments, drainage patterns and lithology at both regional and district scales. The analytical hierarchy process (AHP) approach was used for landslide susceptibility mapping. Several factors such as slope, aspect, soil, lithology, normalized difference vegetation index (NDVI), land cover, distance to drainage, precipitation, distance to fault and distance to the road were extracted from remote sensing satellite data and fieldwork to apply the AHP approach. Directional convolution filters were applied to ALOS-2 data for identifying linear features in particular directions and edge enhancement in the spatial domain. Results indicate that lineament occurrence at regional scale was mainly linked to the N–S trending of the Bentong–Raub Suture Zone (BRSZ) in the west and Lebir Fault Zone in the east of the Kelantan state. The combination of different polarization channels produced image maps that contain important information related to water bodies, wetlands and lithological units. The N–S, NE–SW and NNE–SSW lineament trends and dendritic, sub-dendritic and rectangular drainage patterns were detected in the Kelantan River basin. The analysis of field investigation data indicates that many of flooded areas were associated with high potential risk zones for hydrogeological hazards such as wetlands, urban areas, floodplain scroll, meander bend, dendritic and sub-dendritic drainage patterns, which are located in flat topographic regions. Numerous landslide points were located in a rectangular drainage system that is associated with a topographic slope of metamorphic and quaternary rock units. Consequently, structural and topographical geology maps were produced for Kelantan River basin using PALSAR-2 data, which could be broadly applicable for landslide hazard mapping and identification of high potential risk zone for hydrogeological hazards. Geohazard mitigation programs could be conducted in the landslide recurrence regions and flooded areas to reduce natural catastrophes leading to loss of life and financial investments in the Kelantan River basin. In this investigation, Landsat-8 and ALOS-2 have proven to successfully provide advanced Earth observation satellite data for disaster monitoring in tropical environments.

1 Introduction

The state of Kelantan is located in the northeastern corner of Peninsular Malaysia (Fig. 1). Yearly, several landslides occur during heavy monsoon rainfall in Kelantan River basin. In recent years, in particular, there have been many severe flooding events (in the year 2005, 2006, 2007, 2008, 2009,

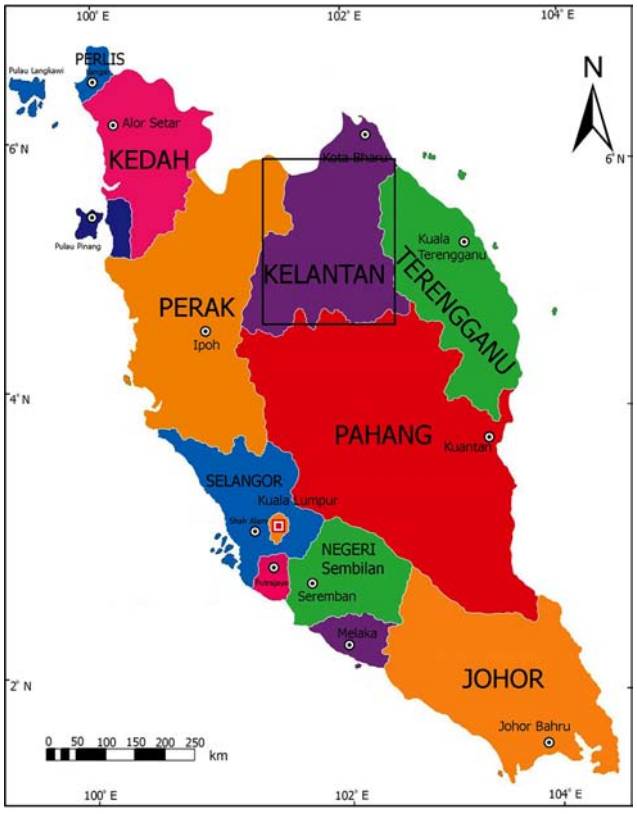

Figure 1. Location of the Kelantan state in Peninsular Malaysia.

2014 and 2015) which have led to significant damage to livestock, agricultural production, homes and businesses in the Kelantan River basin (Pradhan, 2009; Pradhan et al., 2009; Pradhan and Youssef, 2011; Tehrany et al., 2013; Nazaruddin et al., 2014). The problem stems from the inappropriate use of lands that are vulnerable to erosion, quick water runoff and slope failure. Two distinct wet seasons from September to December and February to May are reported by the Malaysian Meteorological Department (MMD) in Peninsular Malaysia (Mardiana et al., 2000). A flood episode in December 2014 caused several landslides, one of which occurred for each kilometer of the area of Kelantan state. Mapping landslides in tropical environments is difficult because landscapes are generally covered by thick tropical rainforest (Plank et al., 2016). In addition, the cloudy weather and rain affected the quality of the optical satellite remote sensing data (Melgani, 2006; Ju and Roy 2008; Ramli et al., 2009; Hashim et al., 2013; Razak et al., 2013; Eckardt et al., 2013; Shahabi and Hashim, 2015). The main target of this investigation is to identify high potential risk and susceptible zones in the Kelantan River basin for mapping landslide occurrence zone using satellite remote sensing technology and geographic information system (GIS) techniques.

Advances in remote sensing technology allow the application of synthetic aperture radar (SAR) data in the geological structural analysis for tropical environments (Shimada and Isoguchi, 2002; Morelli and Piana, 2006; Ramli et al., 2009; Pour and Hashim, 2014, 2015a, b; Pour et al., 2013, 2014). Structural field mapping is often difficult in heavily vegetated terrain. This is the case with the study area where dense vegetation cover, deep weathering and scarcity of bedrock exposure hamper geological structure mapping over a long distance. In addition, the use of optical remote sensing data is limited due to the persistent cloud coverage of the study area for the most part of the year (Ramli et al., 2009; Hashim et al., 2013). SAR data contain the potential to penetrate cloud and vegetation and unlike the optical data are dependent upon the surface roughness of the materials, ideally suited to mapping lineaments (faults and fractures) in tropical environments. Lineaments are related to large structural fractures, which represent zones of weakness in the brittle part of the lithosphere. The presence of linear tectonic structures is one of the most important factors in geological hazard occurrences (Bannert, 2000a, b). Lineaments are represented by faults (linear features), lithological contacts between rock units and drainage patterns in any area (van der Pluijm and Marshak, 1997). Observation from satellite images (Landsat Thematic Mapper) in the Himalayan Mountains of Nepal and China revealed a clear connection between active faults, associated with earthquakes and the occurrence of large landslides (Bannert, 2000a, b). Therefore, delineation of faults and fractures using advanced remote sensing technology in any region is a necessity to assess the potential for many natural geological hazards. Numerous investigations have used faults, drainage patterns and lithology factors as important factors to measure and map the susceptibility of geological hazard (Guzzetti et al., 1999; Dai and Lee, 2002; Suzen and Doyuran, 2004; Abdullah et al., 2013).

Landsat-8 was launched on 4 February 2013, carrying the Operational Land Imager (OLI) and the Thermal Infrared Sensor (TIRS) sensors. These two instruments collect image data for nine visible, near-infrared, shortwave infrared bands and two longwave thermal bands (Irons et al., 2012). They have a high signal-to-noise radiometer performance, enabling 12 bit quantization of data allowing for more bits for better land cover characterization by sharper color contrast. Landsat-8 provides moderate-resolution imagery, from 15 to 100 m of Earth's surface and polar regions (Roy et al., 2014).

The Advanced Land Observing Satellite-2 (ALOS-2) was launched on 24 May 2014, as the successor of ALOS-1 (launched on 24 January 2006 and decommissioned in May 2011) (http://global.jaxa.jp/press/2014/05/20140524_daichi2.html; Blau, 2014). The ALOS-2 is exclusively installed with the Phased Array type L-band Synthetic Aperture Radar-2 (PALSAR-2) using microwaves to maximized its ability compare to the ALOS-1, on which three sensors (one microwave and two optical devices) were on board (Igarashi, 2001; Suzuki et al., 2012).

In particular, L-band microwaves from PALSAR-2 have the ability to penetrate vegetation due to relatively long wavelengths (about 24 cm), making the data particularly useful for geological structural mapping in tropical environments (Igarashi, 2001; Rosenqvist et al., 2004; ERSDAC, 2006; Arikawa et al., 2010; Yamamoto et al., 2013; Pour and Hashim, 2014, 2015a, b; Pour et al., 2013, 2014; Shimada et al., 2015). The wavelength of the L band is relatively long among microwaves (C-band is about 6 cm and X-band is about 3 cm), allowing it to travel all the way down to the ground through vegetation (Woodhouse, 2006). Not only can information be obtained about vegetation but information of the ground surface can be obtained as well. Additionally, the L band is less affected by the growth of vegetation, which is useful for SAR interference analysis (interferometry). Therefore, the L band is capable of acquiring changes on the land more precisely compared to shorter wavelength SAR when some diastrophism takes place due to an earthquake or volcanic activity and floods or landslides caused by a natural disaster (Suzuki, 2014). Accordingly, a further increase in the amount of information for geological structural mapping could be derived from the recently launched PALSAR-2 data. Analysis of the data can provide completely new insights into heavily vegetated areas threatened by natural hazards of geological origin. Consequently, the advanced SAR remote sensing data are broadly applicable for geoenvironmental research to identify the causes of natural disasters and point the way to rehabilitation measures, especially in tropical environments.

In this investigation, multitemporal Landsat-8, the PALSAR-2 data and GIS techniques were integrated to detect and map landslide occurrence zones in the Kelantan state following massive rainfall in December 2014. The specific objectives that drive this investigation are (i) to identify high potential risk and susceptible zones for geological origin hazards using the recently launched ALOS-2 PALSAR-2 remote sensing data in the Kelantan River basin at regional and district scales; (ii) to produce accurate geological structure and topographical maps for the Kelantan River basin using Landsat-8 and PALSAR-2 data; and (iii) to compare the detected high potential risk and susceptible zones with highly damaged areas from recent flooding events in the Kelantan River basin.

The remainder of this paper is organized as follows. Section 2 briefly reviews geology of the Kelantan state. Section 3 explains the characteristics of satellite remote sensing data and their applications in landslide mapping and methodology used in the study. Section 4 describes results and discussion. Finally, Sect. 5 concludes with some accomplishments.

2 Geology of the study area

Peninsular Malaysia forms an integral part of the Southeast Asian continental core of Sundaland and comprises two tectonic blocks/terranes, the Sibumasu Terrane in the west and the Sukhothai Arc in the east, which were assembled by the Late Triassic (Metcalfe, 2013a, b). The state of Kelantan is located in the northeastern corner of Peninsular Malaysia (Fig. 1). Kelantan River is the major river in the region. It appears at the convergence of the Galas River and Lebir River near Kuala Kari and meanders over the coastal plain until it finally degrades into the South China Sea. Kelantan River basin covers 923 km^2, which is about 85 % of the Kelantan state's surface area. It is composed of the flat slope to moderately sloping areas in the northern part and steep scraps and high slopes in the southern part of the river basin (Pradhan et al., 2009). A wide variety of rocks consisting of igneous, sedimentary and metamorphic rocks are distributed in a north–south trend in the Kelantan state. Typically, four types of rocks are classified in the region, including granitic rocks, sedimentary/metasedimentary rocks, extrusive rocks (volcanic rocks) and unconsolidated sediments (Fig. 2). Localized geological features comprise faulting and jointing in the granitic rocks and folding, faulting and jointing in the sedimentary rocks. Granitic rocks are distributed in the west (the Main Range granite) and east borders (the Boundary Range granite) of the state of Kelantan (Rahman and Mohamed, 2001; Department of Minerals and Geoscience Malaysia, 2003; Heng et al., 2006).

The Main Range Granite is located in the west of the state, which is stretched along western Kelantan up to the boundary of Perak and Pahang states and Thailand (Fig. 2). The dominant structural trend in Kelantan is along the N–S to NW–SE direction that derived from post-orogenic phase (Ghani, 2009). The Main Range Granite is located along the western margin of the Bentong–Raub Suture Zone (BRSZ) and extends north to Thailand (Schwartz et al., 1995; Metcalfe, 2000). The north–south-trending Bentong–Raub Suture (approximately 13 km wide) extends from Thailand through Raub and Bentong to the east of Malacca, Peninsular Malaysia. The BRSZ is characterized by a series of parallel topographic north–south-trending lineaments and the presence of small bodies of mafic to ultramafic rocks that are commonly serpentinized (Tan, 1996). The Lebir Fault Zone is located in the eastern part of Kelantan state (Fig. 2), which is one of the major lineaments in Peninsular Malaysia and considered to be post-Cretaceous and a sinistral strike-slip fault (Tjia, 1989; Harun, 2002).

The landscape in the state of Kelantan has been divided into four types: mountainous areas, hilly areas, plain areas and coastal areas (Unjah et al., 2001; Raj, 2009). Mount Chama (Gunung) is the highest point (2171 m) in the Kelantan state, located in Gua Musang district in the western part of the state, near the border of Perak state (Nazaruddin et al., 2014). Quaternary deposits consist of alluvium deposits or unconsolidated sediments. Triassic marine siliciclastics, volcaniclastics, sandstone and limestone are the other sedimentary rocks found in the Kelantan state (Nazaruddin et al., 2014).

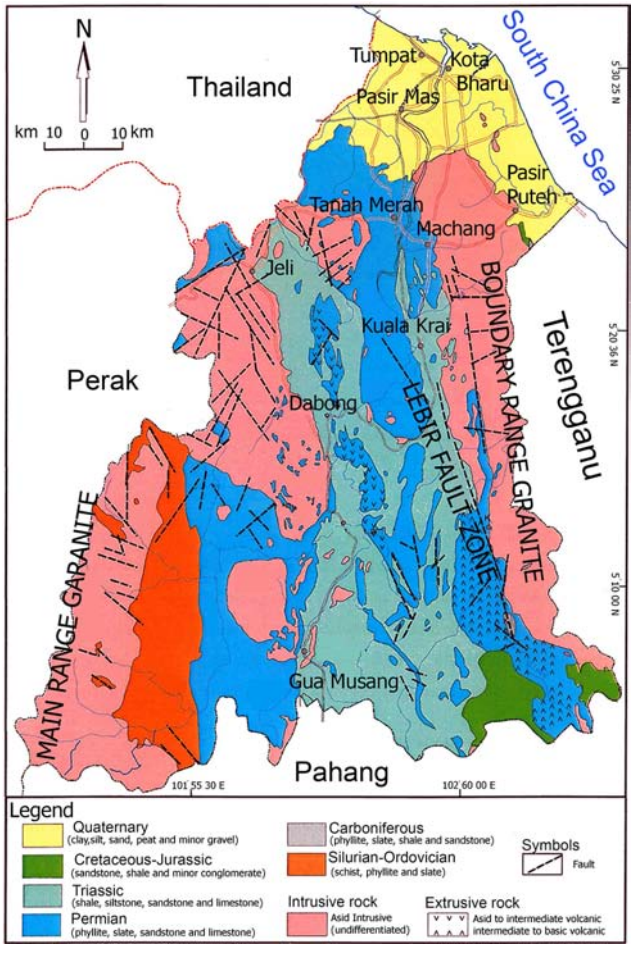

Figure 2. Geologic map of the Kelantan state (modified from Department of Minerals and Geoscience Malaysia, 2003).

3 Materials and methods

3.1 Satellite remote sensing data and characteristics

Landsat-8 and ALOS-2 datasets were used in this study. PALSAR-2 of the ALOS-2 has been significantly improved from ALOS-1's PALSAR in all aspects, including resolution, observation band and time lag for data provision (Arikawa et al., 2010; Kankaku et al., 2010; Suzuki et al., 2012). ALOS-2 science capabilities include global environmental monitoring using the time series PALSAR-2. The research target also covers biospheric, cryospheric and coastal ocean research as well as disaster mitigation (Shimada, 2013). PALSAR-2 is a microwave sensor that emits L-band radio waves and receives their reflection from the ground to acquire information (Suzuki et al., 2012). It has three observation modes, including (i) Spotlight mode, the most detailed observation mode with 1 m by 3 m resolution and observation width of 25 km; (ii) Strip map mode, a high-resolution mode with the choice of 3 m (ultra fine), 6 m (high sensitivity) or 10 m (fine) resolution and observation width of 50 or 70 km; and (iii) ScanSAR mode, a broad area observation width of 350 km (nominal) or 490 km (wide) and resolution of 100 or 60 m (Yamamoto et al., 2013; Shimada et al., 2015). Selection of the most suitable observation mode and time acquisition of PALSAR-2 data for the research objectives will maximize the efficiency of geoenvironmental monitoring works. Two distinct wet seasons from September to December and February to May are reported by the MMD in Peninsular Malaysia (Mardiana et al., 2000). Precipitation and soil moisture variations have an influence on detailed geologic lineament analysis using microwave signal. SAR data are highly sensitive to the water content in the soil because of large contrast between dielectric properties of water and dry soil (Eagleman and Lin, 1976; Jackson and Schmugge, 1989; Lacava et al., 2005). Hence, SAR data acquired during dry seasons contain more useful information for detailed geological structural mapping in tropical environments.

The ScanSAR observation mode has 60 m resolution and 490 km swath width (wide mode), and the fine observation mode contains data with 10 m resolution and 70 km swath width. Dual polarization for the both data includes HH + HV polarization images (HH is horizontally transmitted and horizontally received; HV is horizontally transmitted and vertically received). HV channel is a channel that transmits a vibrating wave in a horizontal direction against the ground (H) and receives it vertically (V). It is expected to acquire more detailed observation data on the ground. Particularly, HV channel (cross polarization) in the ScanSAR and fine observation modes increase the amount of information extraction for geological structural mapping at both regional and districts scales (Pour and Hashim, 2015a, b). HV polarization is more suitable for lineament extraction and edge enhancement in tropical environments than other polarization channels, because cross polarization is more sensitive to lineament and also enhances penetration (Henderson and Lewis, 1998; Pour and Hashim, 2015a, b). Penetration is proportional to wavelength, and cross polarization also enhances penetration (Henderson and Lewis, 1998). Therefore, HV polarization channel records more geological features that are covered by dense vegetation. In the level 3.1 product of PALSAR-2, image quality corrections (noise reduction and dynamic range compression) are performed to level 1.5 PALSAR-2 data. It should be noted that level 1.5 PALSAR-2 data contain the following characteristics: (i) range and multi-look azimuth compressed data are represented by amplitude data, (ii) range coordinate is converted from slant range to ground range and (iii) map projection is also performed (Japan Aerospace Exploration Agency, 2014). The positioning accuracy of PALSAR-2 data is excellent and it does not always require the field survey to modify the positioning accuracy. So, it can reduce the map production time and contribute to cost reduction as well (Shimada et al., 2015).

Two level 1T (terrain-corrected) Landsat-8 OLI images were obtained through the US Geologi-

cal Survey Earth Resources Observation and Science Center (http://earthexplorer.usgs.gov). The image data (LC81270562014339LGN00 and LC81270562015070LGN00) (path/row 127/56) were acquired on 5 December 2014 (before the flooding event) and 11 March 2015 (after the flooding event) with low cloud cover. The image data cover four river basins in Kelantan, including Sungai Golok (103 918.37 ha), Sungai Kelantan (1 308 690.95 ha), Sungai Kemasin (30 927.82 ha) and Sungai Semerak (59 076.48 ha).

In this investigation, a ScanSAR-mode dual polarization (level 3.1; acquired on 6 February 2015) and two fine-mode dual polarization (level 3.1; acquired on 6 February 2015) PALSAR-2 scenes were obtained from ALOS-2 data distribution consortium online system Remote Sensing Technology Center of Japan (RESTEC) (http://www.restec.or.jp/english/index.html) and PASCO Corporation (http://en.alos-pasco.com;https://satpf.jp/) for comprehensive analysis of major geological structures and detailed characterizations of lineaments in the state of Kelantan. The data were processed using the ENVI (Environment for Visualizing Images) version 5.2 and ArcGIS version 10.3 software packages.

3.2 Methods

Atmospheric correction was applied by Fast Line-of-sight Atmospheric Analysis of the Spectral Hypercubes (FLAASH) algorithm on Landsat-8 OLI images. This algorithm contains the standard MODTRAN model atmospheres, which has standard column water vapor amounts for each model atmosphere. Moreover, scene and sensor information (solar zenith angle, satellite view angle and relative azimuth angle between the satellite and the sun) and the aerosol model are considered for running the algorithm (Thome et al., 1998).

Lineaments in remote sensing images have topographic relief and are often a surface expression of 3-D geological structures in the subsurface. Lineaments, associated with brittle and ductile deformation zones, appear as rectilinear and curvilinear patterns in remotely sensed images. Detailed extraction of lineaments helps in reconstructing the tectonic history of a region (Clark and Wilson, 1994). Geological lineament features are attributed to paleotectonic and/or neotectonic activity of a region. The use of remote sensing data in delineation of tectonically significant lineaments has been demonstrated in many geological settings (Raharimahefa and Kusky, 2007, 2009; Amri et al., 2011; Hashim et al., 2013; Hamimi et al., 2014; Pour and Hashim, 2014, 2015a, b; Pour et al., 2014).

Spatial transforms provide reliable and robust image processing techniques to extract the spatial information from remote sensing data. The techniques help to maximize clarity, sharpness and details of features of interest towards information extraction and further analysis. Spatial convolution filtering is based primarily on the use of convolution masks. This flexibility makes convolution one of the most useful tools in image processing. The procedure could be used to enhance low- and high-frequency details, as well as edges in the imagery (Haralick et al., 1987; Jensen, 2005; Schowengerdt, 2007). Linear features are formed by edges of remotely sensed images. Some linear features occur as narrow lines against a background of contrasting brightness; others are the linear contact between adjacent areas of different brightness. Edge enhancement delineates these edges and makes the shapes and details comprising the image more conspicuous and easier to analyze (Jensen, 2005). It can be used in geological applications to highlight rectilinear and curvilinear patterns in remote sensing images.

Systematic image processing techniques were implemented in the PALSAR-2 data for geological structures and lineament mapping at both regional and district scales in the state of Kelantan. It is necessary to treat the speckle in radar images by filtering before it can be used in various applications (Sheng and Xia, 1996). The presence of speckle in radar images reduces the detectability of ground targets, obscures the spatial patterns of surface features and decreases the accuracy of automated image classification (Lee and Jurkevich, 1994; Sveinsson and Benediktsson, 1996). However, image quality corrections (noise reduction) have been already applied to level 3.1 product of PALSAR-2, but some speckles (salt and pepper noise) could still be seen in the images. In this study, the median spatial convolution filter was used for noise removal and smoothing the PALSAR-2 images. The median filter is a particularly useful statistical filter in the spatial domain, which effectively remove speckle (salt and pepper noise) in radar images without eliminating fine details (Russ, 2002; Research Systems, Inc., 2008). The median operation has the effect of excluding pixels that do not fit the typical statistics of the local neighborhood, i.e., outliers. Isolated noise pixels can, therefore, be removed with a median filter (Schowengerdt, 2007). The median filter is especially useful for removing shot noise (pixel values with no relation to the image scene) and has certain advantages, such not shifting boundaries and minimal degradation to edges (Eliason and McEwen, 1990; Russ, 2002; Jensen, 2005). In this study, a 3×3 neighborhood convolution mask (kernel) was applied to the PALSAR images. Image Add Back value was entered at 60 %. The Image Add Back value is the percentage of the original image that is included in the final output image. This part of the original image preserves the spatial context and is typically done to sharpen an image.

The directional nature of geological lineaments accentuates the need for directional filtering to obtain maximum structural mapping efficacy. Edge enhancing filter highlights any changes of gradient within the image features such as structural lines (Tripathi and Gokhale, 2000). A linear filter is calculated in the spatial domain as a weighted sum of pixels within the moving window. This discrete convolution between the input image f and the window response func-

tion w, both of size $N_X \times N_Y$, is written mathematically for the output pixel gij as

$$gij = \sum_{m=0}^{N_x-1} \sum_{n=0}^{N_y-1} f_{mn} w_{i-mj-n} \quad (1)$$

and expressed symbolically in the convenient form of

$$g = f \cdot w. \quad (2)$$

Since the nonzero extent of the window is typically much smaller than the image, the sum in Eq. (1) does not have to be over every pixel. If the window is $w_x \times w_y$ pixels, we can write an alternate expression:

$$gij = \sum_{m=i-W_y/2}^{i+W_y/2} \sum_{n=j-W_x/2}^{j+W_x/2} f_{mn} w_{i-mj-n}, \quad (3)$$

where w is centered at (0, 0) and is nonzero over $\pm w_{x/2}$ and $\pm w_{x/2}^2$. In this form, we can clearly see that the output pixel is a weighted sum of pixels within a neighborhood of the input pixel. The distinguishing characteristic of a linear filter is the principle of superposition, which states that the output of the filter for a sum of two or more inputs is equal to the sum of the individual outputs that would be produced by each input separately. This is achieved with a convolution because Eq. (2) is a linear weighted sum of the input pixels. Furthermore, the filter is shift-invariant if the weights do not change as the window moves across the image (Schowengerdt, 2007).

Directional filters are used to enhance specific linear trends in an image. A typical directional filter consists of two kernels, each of which is an array of three by three pixels. The left kernel is multiplied by the $\cos A$, where A is the angle, relative to the north, of the linear direction to be enhanced. The right kernel is multiplied by $\sin A$. Angles in the northeastern quadrant are considered negative; angles in the northwestern quadrant are positive. The filter can be demonstrated by applying it to a dataset in which a brighter area is separated from a darker area along a total lineament that trends northeast ($A = -45°$) (Carr, 1995; Sabins, 1996; Vincent, 1997; Research Systems, Inc., 2008).

In this study, for identifying linear features in particular directions and edge enhancement in the spatial domain, directional convolution filters were applied to the median resultant image. Directional filtering technique is a straightforward method for extracting edges in the spatial domain that approximate the first derivative between two adjacent pixels. The algorithm produces the first difference of the image input in the horizontal, vertical and diagonal directions (Haralick et al., 1987; Carr, 1995; Sabins, 1996; Vincent, 1997; Jensen, 2005). As a result, many additional edges of diverse orientations are enhanced (Richard and Jia, 1999). The edges appear as a plastic shaded-relief format (embossing) in the image because of the 3-D impression conveyed by the filtering (Schowengerdt, 2007). The directional filter is used for producing artificial effects suggesting tectonically controlled linear features (Pour and Hashim, 2015a, b).

Directional filters were used to enhance specific linear trends in the median resultant image. Four principal directional filters, N–S, E–W, NE–SW and NW–SE with 5×5 and 7×7 kernel sizes, were applied to ScanSAR and fine scenes, respectively. A 5×5 kernel matrix was selected for ScanSAR scene to enhance rough/smooth and semi-rough features at a regional scale in the northern part of Peninsular Malaysia. A 7×7 kernel matrix was applied to fine scenes for enhancing semi-smooth and smooth/rough features at district scale in the Kelantan state (Chavez and Bauer, 1982; Jensen, 2005). Directional filter angles were adjusted as N–S (0°), E–W (90°), NE–SW (45°) and NW–SE (135°). North (up) is 0° and the other angles are measured in a counterclockwise direction. An Image Add Back value of 60 % was entered.

Landslide is triggered by two forces, namely "precondition factors" that govern the slope stability and "preparatory and triggering factors" (Komac, 2006). In this study, landslides caused by heavy flooding episodes in the Kelantan state in December 2014 were reported as (i) a large-scale landslide ($> 300\,m^2$) that could be detected by satellite remote sensing data and (ii) a small-scale landslide ($< 300\,m^2$) that measured and determined during a scientific expedition in the Kelantan River basin between 20 and 25 January 2015. Data collection in landslide-affected zones and flooded areas has been done by Global Positioning System (GPS) surveying. GPS surveying was carried out in the Tanah Merah, Machang, Jeli, Kuala Krai and Gua Musang districts in the Kelantan River basin using a Garmin® MONTERRA® with an average accuracy 5 m in 453 landslide-affected location points. These locations were recorded in a forest, rubber trees, bushes (degraded forest), mixed crops, oil palm, cleared land, urban area and agriculture lands.

In the Landsat-8 OLI images, landslides were determined by tracking changes in vegetation pixel data using Landsat-8 images acquired before and after flooding. The normalized difference vegetation index (NDVI) was calculated using infrared and red bands of Landsat-8 datasets.

$$\mathrm{NDVI_{OLI}} = (\mathrm{Band5_{OLI}} - \mathrm{Band4_{OLI}}) / (\mathrm{Band5_{OLI}} + \mathrm{Band4_{OLI}}), \quad (4)$$

where $\mathrm{Band5_{OLI}}$ is reflectance unit of near-infrared-band Landsat-8 OLI and $\mathrm{Band4_{OLI}}$ is reflectance unit of red-band Landsat-8 OLI.

In this investigation, the analytical hierarchy process (AHP) approach was used for landslide susceptibility mapping (LSM). The AHP is a multi-objective, multi-criteria decision-making approach that enables the user to arrive at a scale of preferences drawn from a set of alternatives (Saaty, 1980; Saaty and Vargas, 1991, 2001). AHP involves building a hierarchy of decision elements (factors) and then making comparisons between possible pairs in a matrix to give a weight for each element and also a consistency ratio. It is

Table 1. Pair-wise comparison matrix for each input of AHP.

Factor	Slope	Aspect	Soil	Lithology	NDVI	Land cover	Precipitation	Distance to road	Distance to river	Distance to fault
Slope	0.032	0.031	0.029	0.018	0.030	0.034	0.023	0.060	0.014	0.014
Aspect	0.032	0.031	0.036	0.070	0.030	0.021	0.015	0.050	0.014	0.014
Soil	0.161	0.123	0.145	0.175	0.075	0.206	0.226	0.150	0.170	0.211
Lithology	0.065	0.015	0.029	0.035	0.050	0.026	0.015	0.060	0.019	0.021
NDVI	0.161	0.154	0.291	0.105	0.150	0.206	0.090	0.100	0.226	0.211
Land cover	0.097	0.154	0.073	0.140	0.075	0.103	0.135	0.100	0.170	0.169
Precipitation	0.065	0.092	0.029	0.105	0.075	0.034	0.045	0.060	0.019	0.021
Distance to road	0.161	0.185	0.291	0.175	0.499	0.309	0.226	0.300	0.283	0.211
Distance to river	0.129	0.123	0.048	0.105	0.037	0.034	0.135	0.060	0.057	0.085
Distance to fault	0.097	0.092	0.029	0.070	0.030	0.026	0.090	0.060	0.028	0.042
Sum	1.000	1.000	1.000	1.000	1.000	1.000	1.000	1.000	1.000	1.000

based on three principles: decomposition, comparative judgment and synthesis of priorities (Malczewski, 1999). To apply this approach, it is necessary to break a complex unstructured problem down into its component factors, arrange these factors in a hierarchic order, assign numerical values to subjective judgments on the relative importance of each factor and synthesize the judgments to determine the priorities to be assigned to these factors (Saaty and Vargas, 2001; Yalcin, 2008; Yalcin et al., 2011; Choi et al., 2012).

In this investigation, to apply the AHP approach, 10 factors – slope, aspect, soil, lithology, NDVI, land cover, distance to drainage, precipitation, distance to fault and distance to the road – were extracted from Landsat-8 images, PALSAR data and fieldwork as shown in Fig. 3. Comparisons between the 10 factors show that slope, land use type, distance to the fault line and precipitation intensity are more important than the others. A scale of numbers is crucial to indicate how many times more important or dominant one element is over another element with respect to the criterion or property to which they are compared. The relationships between the detected landslide locations and these 10 related factors were calculated based on AHP procedure and prior knowledge (Tables 1 and 2). The distance between detailed fault line derived from PALSAR-2 data and all landslides point was computed in ArcMap 10.3 software using Euclidean distance.

Among selected 10 factors as the input of the AHP approach, it seems that the excessive rainfall during December 2014 flood episode in the Kelantan is more significant than than the other nine parameters. Thus, rainfall analysis was carried out based on daily precipitation from about 80 stations before and during December 2014 flood episode in the Kelantan state. Table 3 shows rainfall amount for each district in Kelantan state. The rainfall analyses for 452 landslide events were carried out to define the threshold rainfall intensity triggers landslides to occur. All data from rain gauge were extracted to obtain the average rainfall intensity

Table 2. Factor weights for each input of AHP.

Factors	Weight
F1: precipitation	0.141
F2: slope	0.123
F3: soil	0.121
F4: aspect	0.102
F5: lithology	0.097
F6: land cover	0.086
F7: distance to road	0.084
F8: distance to drainage	0.081
F9: NDVI	0.073
F10: distance to fault	0.062

of the whole year of 2014 and to compute the anomaly of rainfall amount during the flood episode. The pre-occurrence of the next landslides could be predicted by determination of a threshold value of the rainfall intensity in Kelantan that triggers the slope failure to occur. Most landslide events reported during and after the flood episode occurred during the rainy season. The relationship between absolute antecedent rainfall precipitation and landslide occurrence was studied by using a general methodology for statistical analysis of landslide induced by rainfall based on the reconstruction of absolute antecedent precipitations. Equation (2) was used to obtain the spatial distribution of the landslide susceptibility map of each class during and before flood episode in Kelantan 2014.

$$\mathrm{LSM} = \sum_{i=1}^{n} (R_i W_i), \tag{5}$$

where R_i represents the rating class for each and every layer where W_i is the weight for the landslide factors. After getting the result of LSM, it is then be divided into five different classes labeled as low risk (LS), fair risk (FS), medium susceptibility (MS), high risk (HS) and very high risk (VHS) based on the natural break method.

Table 3. Rainfall amount for each district in Kelantan.

District	Width (km^2)	Rainfall amount during flood episode (mm)	Percentage of rainfall in flood episode (%)	Annual rainfall amount (mm)	Percentage of annual rainfall (%)
Tumpat	169.50	1558.70	10.44	3621.28	6.40
Kota Bharu	115.64	3054.00	20.45	1764.10	10.75
Pasir Puteh	433.80	4783.50	32.03	1434.72	13.55
Tanah Merah	884.14	5527.30	37.01	1996.58	15.76
Jeli	1330.48	5132.20	34.37	348.18	9.62
Kuala Krai	2329.00	3091.10	20.70	2023.65	9.64
Gua Musang	8214.30	9584.10	64.19	922.03	24.31
Machang	546.26	1469.00	9.84	1605.00	2.33
Pasir Mas	139.00	2402.20	16.01	1407.86	9.42

4 Results and discussion

A wide-swath ScanSAR observation mode of PALSAR-2 was used for comprehensive analysis of major geological structures, which shows mega-geomorphology and mega-lineaments in the Kelantan state. Figure 4 shows an RGB color composite of HH polarization channel in red, HV polarization channel in green and HH + HV polarization channel in blue for the ScanSAR resultant image. The RGB color composite yields an image with great structural details and geomorphological information. The different colors in the image indicate different backscattering signals from the ground. The Main Range granite located in the western part of the image and the Boundary Range granite on the eastern borders of Kelantan state appear as light green to green in color, which shows the regions with high altitude in the scene (Fig. 4). Major transcrustal lineaments such the BRSZ and Lebir Fault Zone are also detected. Quaternary deposits, Triassic marine siliciclastics, volcaniclastics, sandstone and limestone are manifested as pink to purple tones consisting of lands with low elevation (Fig. 4). Lakes and main river systems are portrayed as blue to dark blue in the image. In fact, the lines range from blue to dark blue on the image are faults and fracture zones occupied by streams. The river pattern is one of the most important factors contributing to the lineament because it reflects the nature of the existing fracture system (Suzen and Toprak, 1998).

Figure 5 shows a ScanSAR HV polarization image that is superimposed on a general topography map of the Kelantan state (Department of Minerals and Geoscience Malaysia, 2003). It is evident that the morphology of the study area is largely controlled by rock type and structure. High-elevation areas (500–100 and < 1000 m) in the Kelantan state are mountainous areas associated with Main Range granite (in the west) and Boundary Range granite (in the east). Hilly, plain and coastal areas with an altitude between 500 and 50 m are associated with sedimentary rocks.

Figure 6 shows the resultant image map for N–S, NE–SW and NW–SE (R: 0°; G: 45°; B: 135°) directional filters. A major change in deformation style is obvious from the west to the east in Fig. 6. Structural analysis reveals four distinct parts from the west to the east, including (i) western part of the scene by ductile fabrics, (ii) western of the BRSZ affected mainly by brittle deformation, (iii) ductile–brittle deformation between the BRSZ and Lebir Fault Zone and (iv) brittle–ductile fabrics between Lebir Fault Zone and eastern coastal line. Lineament occurrence in Fig. 6 is mainly linked to the N–S trending of the BRSZ and Lebir Fault Zone. Generally, major faults are strike-slip with both dextral and sinistral movements, which trend N–S and NW–SE. NW–SE-trending strike-slip faults moved sinistrally in the Lebir Fault Zone. The sinistral movement along the Lebir Fault Zone is responsible for the formation of folding and reverse faulting adjacent to the fault and surrounding area. These structures characterized transpressive tectonic regime in Peninsular Malaysia (Richter et al., 1999; Harun, 2002).

The collision zone and compressional structures appear clearly in the west of the BRSZ in Main Range granite (Fig. 6). Deformation in this region shows the shortening zone oriented parallel to the BRSZ. Several faults, joints and fractures represent brittle deformation events in the region that mostly strike NW–SE. Generally, most of the short lineaments are clustered in the collision zone. Ductile deformation in the western margin of the image (Fig. 6) includes upright asymmetrical mega-folds with axial surfaces oriented W–E. Hence, the contractional strain direction affected by this domain is from NE–SW, followed by dextral shearing. The deformed area zone between the BRSZ and Lebir Fault Zone represents fault systems and folding area. NW–SE striking strike-slip faults and NE–SW normal faults are dominated brittle structural elements within this domain. Ductile defor-

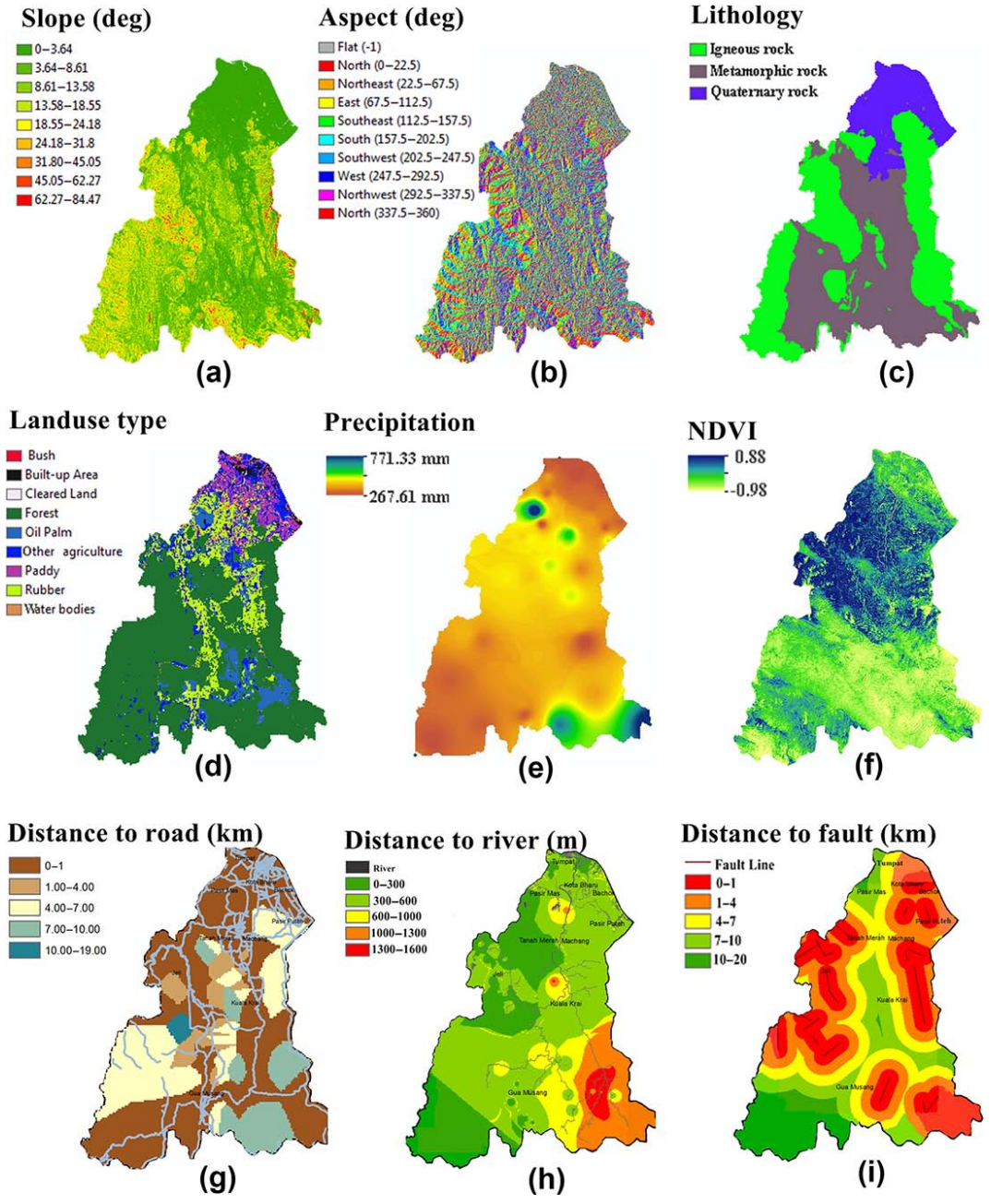

Figure 3. List of extracted factors from Landsat-8, PALSAR and fieldwork: **(a)** slope (degree), **(b)** aspect (degree), **(c)** lithology types, **(d)** landuse type, **(e)** precipitation (mm), **(f)** NDVI, **(g)** distance to main road, **(h)** distance to main river (m) and **(i)** distance to fault line (km).

mation is demonstrated by several open upright folds, which have W–E to NE–SW axial plans (Fig. 6). Brittle–ductile fabrics in the eastern part of the image between Lebir Fault Zone and eastern coastal line illustrate curved shear zone that occupied several N–S and NW–SE striking faults, fractures and joints. A mega-concentric fold surrounds the shear zone with a WE striking axial surface. According to the orientation of the lineaments, sinistral movement along the Lebir Fault Zone has generated the tectonic features. Some N–S and NE–SW-trending normal faults and small curvatures are also identifiable near the eastern coastal line (Fig. 6).

Figure 7 shows a fine-mode merged image of the northern and southern parts of the Kelantan state. In this figure, HH polarization channel was assigned to be red, HV polarization channel to be green and HH + HV polarization channels to be blue for generating an RGB image for the study area. This color combination produced an image map contains important information related to water bodies, wetlands and ge-

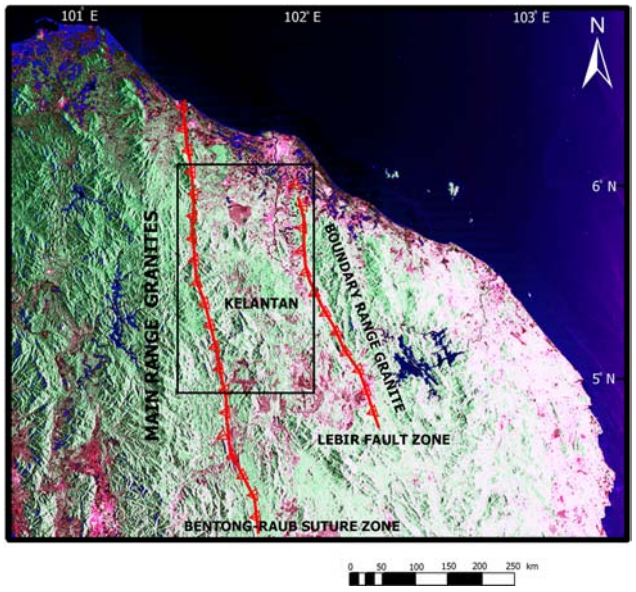

Figure 4. RGB color combination (HH, HV and HH + HV polarization channels) of PALSAR-2 Scan SAR scene covering the northern part of the Peninsular Malaysia. Black rectangle shows the selected area for detailed analysis using fine-mode images of the northern and southern parts of the Kelantan state in this study.

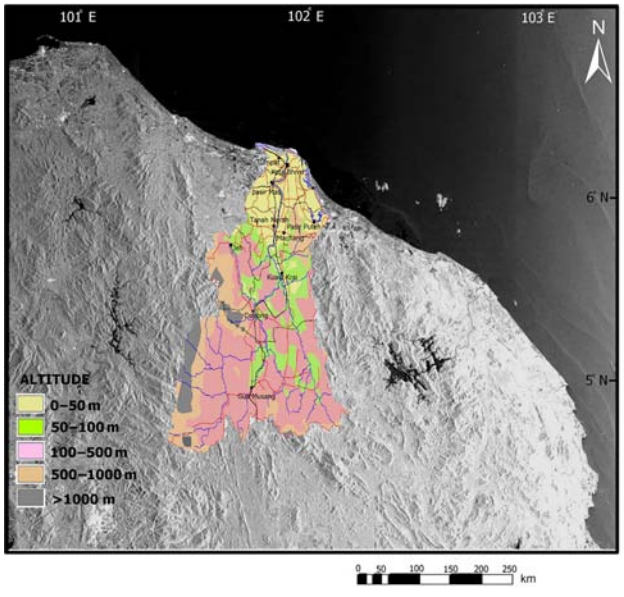

Figure 5. ScanSAR HV polarization image of the Kelantan state superimposed by general topography map.

ological structural features. River systems and lakes appear black especially in the northeastern part of the image and wetlands as mauve (Fig. 7). Smooth surfaces such as calm water bodies appear dark in SAR images due to the reflection of the radar signal. Hence, no returning radar signal could be detected in receiving antenna (Thurmond et al., 2006; Pour

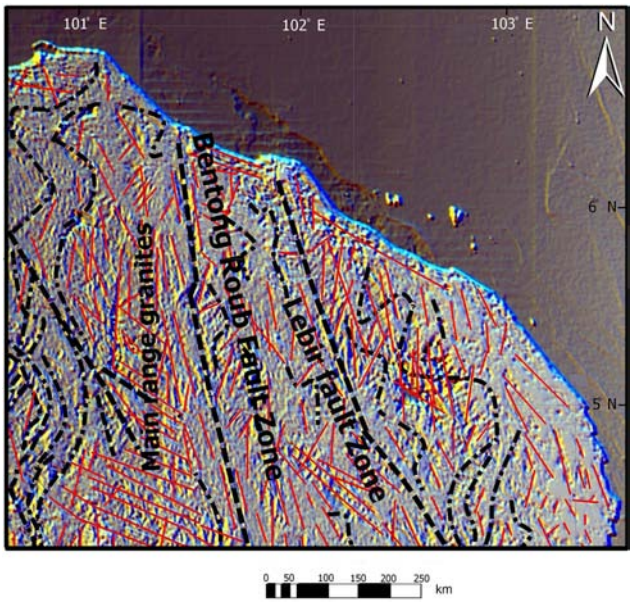

Figure 6. ScanSAR image map derived from N–S (0°), NE–SW (45°) and NW–SE (135°) directional filters for the northern part of the Peninsular Malaysia. The explanation for the figure: dashed black lines are major faults; dot-dashed lines are folds and curvilinear; red lines are faults and fractures.

and Hashim, 2015a). Besides, the best soil moisture/wetness information is achievable from L-band microwaves because it comes out from deeper soils. In fact, vegetation is almost transparent and roughness effects are negligible using L-band microwaves for soil wetness mapping/monitoring (Jackson and Schmugge, 1989; Lacava et al., 2005). Soil moisture is one the most important factors in hydrogeological hazards, especially since the soil response is affected by its status of saturation. Accordingly, the identification of wetlands is very important for flood forecasting and prevention in the state of Kelantan. Wetlands are more distributed in the northern part of the study area (Fig. 7). A vast wetland (dark mauve) is represented clearly in the central north segment of the image. Several wetlands, such as light to dark mauve, are observable in central-east, south and southwestern part of the image (Fig. 7).

The RGB image map (Fig. 7) was compared with the geological map of the Kelantan state. It is evident that most of the detected wetlands are associated with sedimentary and metamorphic rocks. A few of the wetlands are located in the granite bedrock areas in the west (the Main Range Granite) and east (the Boundary Range granite) of the state of Kelantan. The granite bedrock areas are all characterized by dissected hilly to mountainous terrain that gives rise to isolated highlands and mountain ranges (Fig. 7). These granitic areas represent the outcrops of a number of granite batholiths that are generally elongated along a N–S to NNW–SSE direction (Bignell and Snelling, 1977).

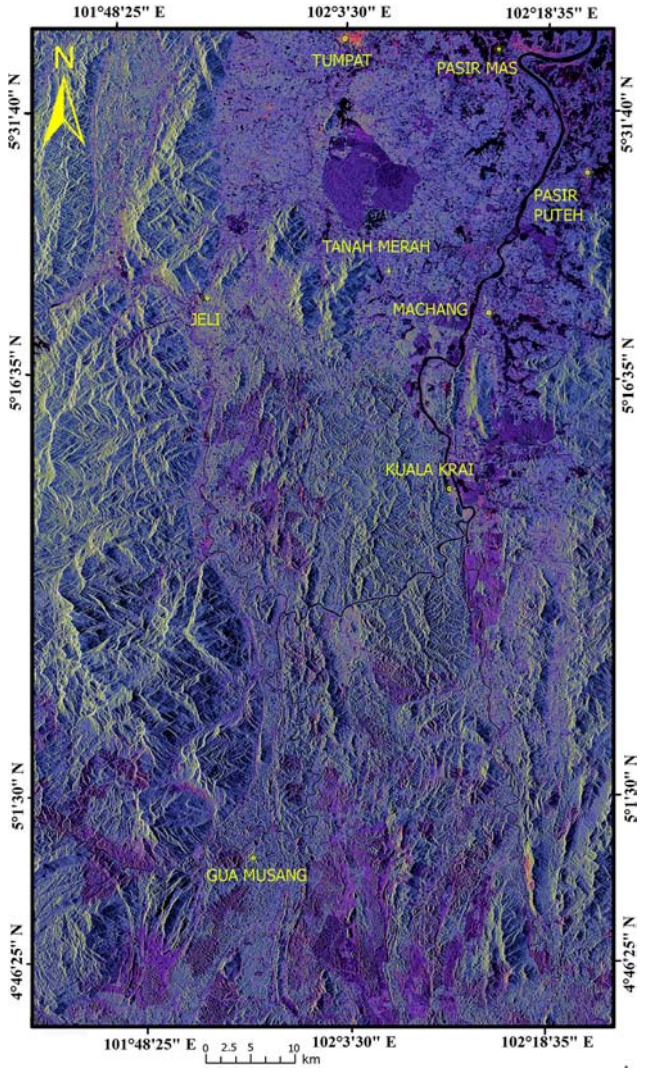

Figure 7. RGB color composite image of HH, HV and HH + HV polarization channels derived from fine-mode merged image of the northern and southern parts of the Kelantan state.

LSMs for before and after flood episodes were produced using related factors contributing to landslides event in the Kelantan state (Fig. 8). Overall, the number of landslides was 452. About 36.7 % occurred in the area of rubber plantation area, while 34.3 % occurred in forest areas. Location of landslides occurrences at different land use/cover type in Kelantan is given in Fig. 9. Forest is the dominant land use/cover in Kelantan besides rubber and palm oil.

The amplitude of the radar signal is highly sensitive to the physical properties of the ground surface, which produces the brightness of the surface to vary much more than optical or infrared images (Robinson et al., 1999). Hence, a combination of different polarization channels of fine-mode PALSAR-2 data contains considerable information for rock discrimination. In this study, an RGB color composite was produced by assigning HV + HH polarization channels to red, HV/HH polarization channels to green and HV polarization channel to blue for detailed rock discrimination in the Kelantan state. Figure 10 represents the RGB merged image for the northern and southern parts of the Kelantan state. Granitic rocks are manifested as light green (dark green in high-altitude area probably due to layover effect on SAR image; Gelautz et al., 1998; Franceschetti and Lanari, 1999), while sedimentary and metamorphic rocks appear as a variety of tones such as brown, light brown, dark green, light blue and light red in the image (Fig. 10). In comparison with the geological map of the study area, it seems that brown and dark green hues are metamorphic rocks and light brown, light blue and light red are sedimentary rocks (clay, shale, conglomerate, sandstone and limestone). River systems and lakes are observable clearly as black meandering streams and water bodies especially in the northern segment of the region (Fig. 10).

Four directionally filtered images of fine-mode observation, which contain enhanced information for a set of lineaments in N–S, E–W, NE–SW and NW–SE directions, were used for lineament mapping in the Kelantan state. Figure 11a shows a structural map for the Kelantan state, which is derived from the resultant image of directional filtering to HV polarization channel. It should be noted that the locations of wetlands are also portrayed in this figure. The most important structural features in the image map are fault zones, river systems and drainage lines patterns (Fig. 11a). Within the study area, two large fault zones are presented: BRSZ in the northwest and Lebir Fault Zone in the southeast. The N–S, NE–SW and NNE–SSW lineament trends are commonly dominant in the image map. The dominant lineaments tend to run in the N–S direction, which is mainly linked to the N-S trending of the BRSZ (in the west) and Lebir Fault Zone (in the east). Additionally, few short NW–SE-trending lineaments are detected in the western and eastern parts of the study area (Fig. 11a). The N–S and NE–SW striking system distributed in the southeastern segment of the region is particularly related to Lebir Fault Zone. The pattern of the lineament map in the northwestern part of the image map displays the occurrence of BRSZ, which contains lineaments in N–S and NNE–SSW directions. Most of the short and smaller faults follow the N–S, NE–SW and NNE–SSW trends as the major fault systems in the Kelantan state. It seems that the NW–SE faults are the youngest faults in the study area due to the low frequency of lineaments in this trend. The major N–S-trending faults are interpreted as oldest structures in Peninsular Malaysia and related to the amalgamation of Gondwana-derived terranes during the Permian–Triassic, and NE–SW and NW–SE-trending faults are interpreted to be Late Triassic to Jurassic in age (Metcalfe, 2013b).

The occurrence and concentration of geological structural features in any region are related to rock type, thickness of uppermost weathered mantle and brittleness of rocks (Harris et al., 1960). In the Kelantan state, high concentrations of lin-

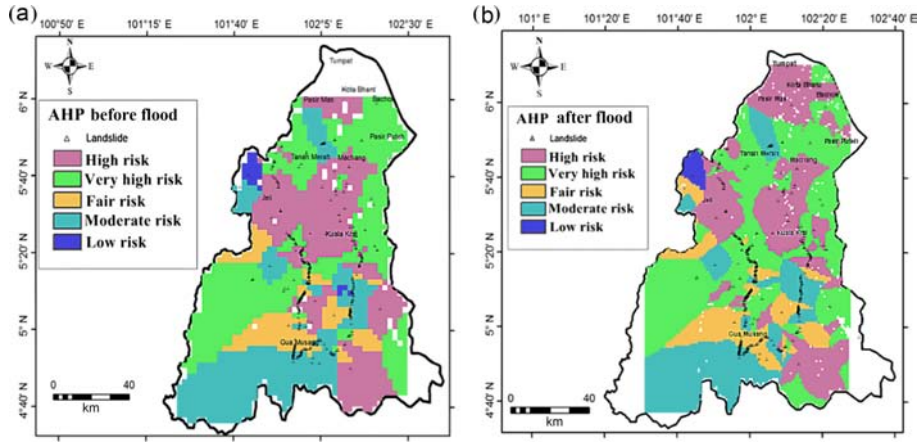

Figure 8. LSM before **(a)** and after **(b)** 2014 flooding episode in Kelantan state.

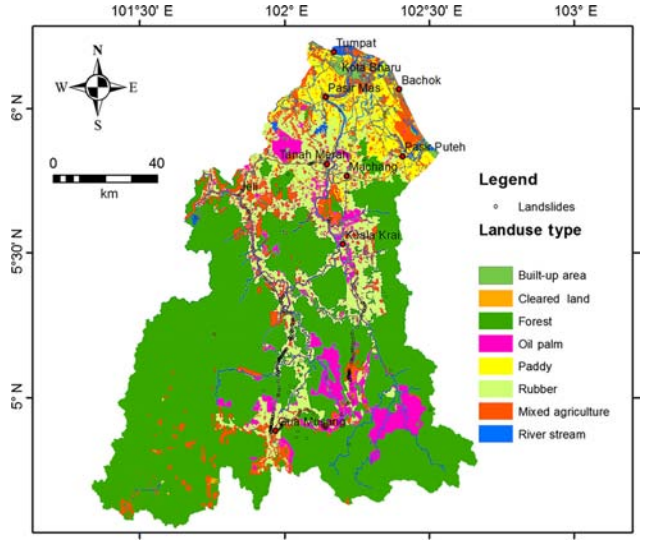

Figure 9. Land use/cover map of the Kelantan state.

eaments are associated with granitic rocks in higher terrains and low concentrations of lineaments are usually associated with lower terrains of metamorphic and sedimentary rocks. Tjia and Harun (1985) analyzed regional structures of Peninsular Malaysia and reported that many lineaments are very well displayed in areas underlain by granite, whereas in other areas they are poorly shown. Moreover, Akhir (2004) identified that high lineament concentrations in the Upper Perak Valley, Perak state, Peninsular Malaysia are closely related to higher terrain which is formed by more-resistant rocks such as granite and sandstone, whereas low lineament concentrations are associated with lower terrain which is mainly formed by less-resistant rock types such as shale and slate. As well, volcanic rocks in the Upper Perak Valley encompass a low lineament concentration (Akhir, 2004).

The rivers in the study area are structurally controlled. They display zigzag patterns due to the presence of fractures, joints and faults with changes in orientation (Fig. 11a). The drainage system in the Kelantan River basin shows dendritic, sub-dendritic and rectangular patterns (Fig. 11a). It is evident that the drainage pattern is apparently being controlled by structure and lithology in the study area. However, several factors such as topography, soil type, bedrock type, climate and vegetation cover influence input, output and transport of sediment and water in a drainage system. The geological structures and lithologic variation have given rise to different drainage patterns (Summerfield, 1991). For instance, a dendritic and sub-dendritic pattern with a large number of tributaries is typical of drainage in areas of impermeable crystalline rock such as gneiss and/or sediment of uniform resistance (horizontal strata). The pattern is characteristic of essentially flat-lying and/or relatively homogeneous rocks and impervious soils with the lack of structural control. A rectangular pattern is usually caused by jointing or faulting of the underlying bedrock. It is usually associated with massive, intrusive igneous and metamorphic rocks (Summerfield, 1991). Therefore, it is assumed that the area with the dendritic and sub-dendritic pattern is subjected to hydrogeological hazards such as flooding because of low infiltration runoff. Rectangular drainage pattern is a susceptible zone that could be easily affected by landslide due to the slope of the land, lithostructural conditions and speed of runoff. In the Kelantan River basin, most of the dendritic and sub-dendritic drainage patterns are detected in central part of the river basin (Fig. 11a), which consists of sedimentary rocks. However, most of the rectangular drainage patterns are associated with igneous and metamorphic rocks in the western part of the Kelantan River basin (Fig. 11a). A structural and topographical feature map of the Kelantan River basin is shown in Fig. 11b. It is evident that most of the dendritic and sub-dendritic drainage patterns are located in lowlands and the rectangular drainage pattern dominates in highlands in the Kelantan River basin.

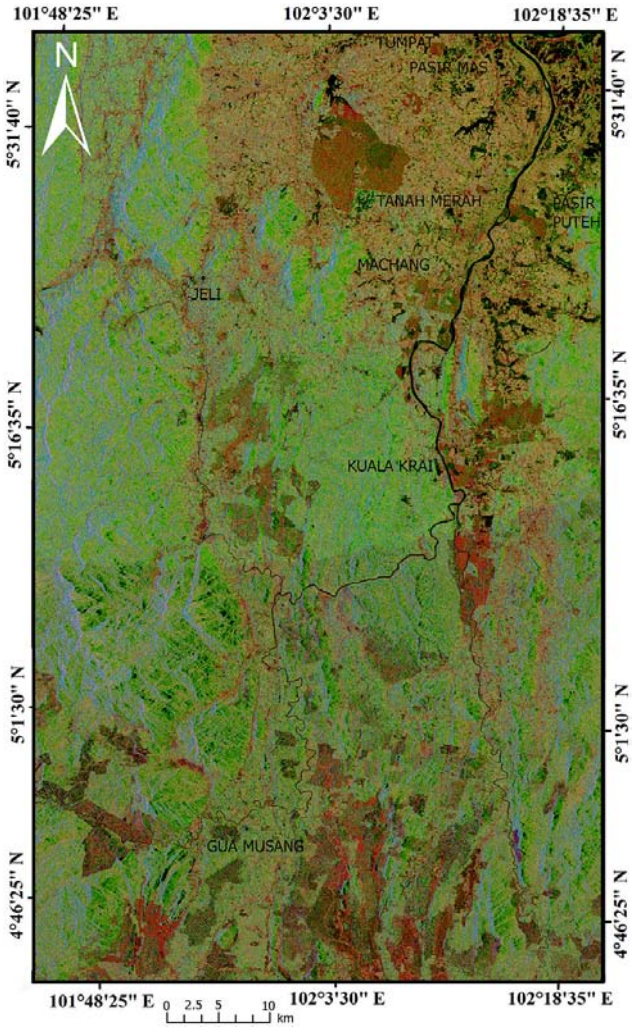

Figure 10. RGB color composite image of HV + HH, HV/HH and HV polarization channels derived from fine-mode merged image of the northern and southern parts of the Kelantan state.

Precipitation influences the occurrence of landslides more than the distance to fault, which can be seen as having the lowest impact on landslide susceptibility. According to the landslide susceptibility map, 65 % of the whole area of Kelantan is found to be under the category of a low landslide susceptibility zone, while 35 % class located within high susceptibility zone. Table 4 shows information on statistical testing of landslides due to rainfall amount for the Kelantan state during the December 2014 flood episode. Two assumptions were used for statistical testing of the landslide in this analysis: (a) the value of rainfall is one of the major factors contributing to the landslide tragedy in Kelantan, which is assumed to be H_0, and (b) the value of rainfall is *not* the major factor contributing to the landslide tragedy in Kelantan, which is determined to be H_A. The ANOVA test shows that F calculated $< F$ significance; thus the null hypothesis is accepted. The test statistic is the $F_{\text{statistic}}$ value of 0.0938. Using α of 0.05, $F_{0.05;1,97} = 3.939$. Since the $F_{\text{statistic}}$ value is much smaller than the critical value (p value $= 0.7601$), thus the null hypothesis, H_0 is accepted at equal rainfall means and conclude that rainfall is one of the major factors contributing to the landslide tragedy in the Kelantan.

Before the flood, the mean amount of rainfall is much lower than mean of rainfall during flood episode, where few landslide points during 2014 fall under the mean of normal rainfall. During the flood episode, as the mean of rainfall is very high, many landslides points fall higher than the mean value. It is evident that a landslide is triggered when the amount of average monthly rainfall reaches ± 400 and ± 800 mm for daily rainfall.

Further analysis has been carried out after the detection of landslides in Kelantan state and landslide susceptibility mapping through the GIS-based statistical model. Since the landslides occur mainly in the forest, information about what density of trees will cause slope failure is crucial any mitigating action plan to be undertaken in the future by the local authorities. Thus, ground surface displacement for all identified landslides occurrences and relation to forest density should be carried out. To know the impact of a landslide event that shifts the variety of different density of forest in an affected area, the area of the landslide before and after a flood episode must be analyzed by associating its size with forest density. Stock plots indicate that before a rainy season (Fig. 12a) many landslides in Kelantan tend to occur in moderate forest density (close to 0.50 NDVI value), while landslides are more likely to occur at a location with a slightly lower NDVI value (almost 0.40) during the flood episode (Fig. 12b). In contrast, large landslides are not highly dependent on how dense the forest is but are more likely due to other factors such as slope failure, geological structures (faults and fractures) and heavy rainfall.

Field observations were conducted to compare the detected high potential risk and susceptible zones with highly damaged areas in recent flooding events in the Kelantan River basin. The analysis of field investigation data indicates that many of flooded areas were associated with high potential risk zones for hydrogeological hazards such as wetlands, urban areas, floodplain scroll, meander bend and dendritic and sub-dendritic drainage patterns. Most of the hydrogeological hazards zones are located in flat topographic regions. Flat topography with impervious soils/surface has low infiltration runoff, which yields more storm runoff during heavy monsoon rainfall compared to other regions. Figure 13a and b show meander bends and floodplain scroll zones in the Kelantan River basin, which were flooded areas during the 2015 flooding event.

Numerous landslide-affected points were recorded in the high-altitude segment of the south and southwestern part of the Kelantan state. As mentioned above, high drainage density of the rectangular system is governed in this domain. The drainage density affects runoff, in that a high drainage density drains runoff water rapidly, decreases the lag time

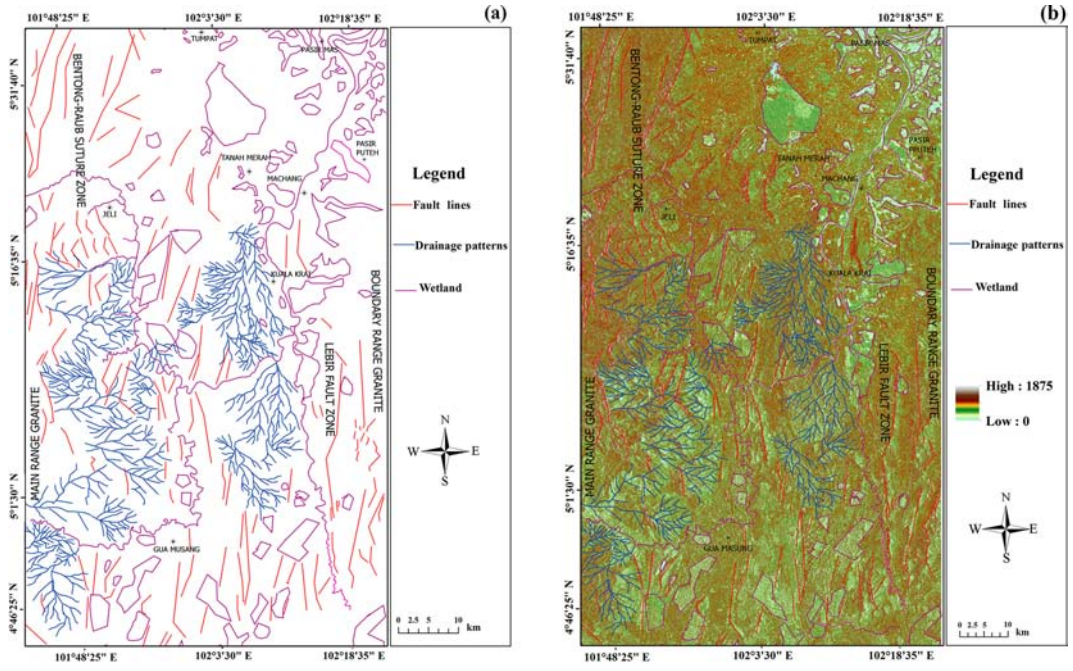

Figure 11. **(a)** Structural lineament map of the Kelantan state derived from directional filtering to HV polarization channel. **(b)** Structural and topographical feature map of the Kelantan River basin.

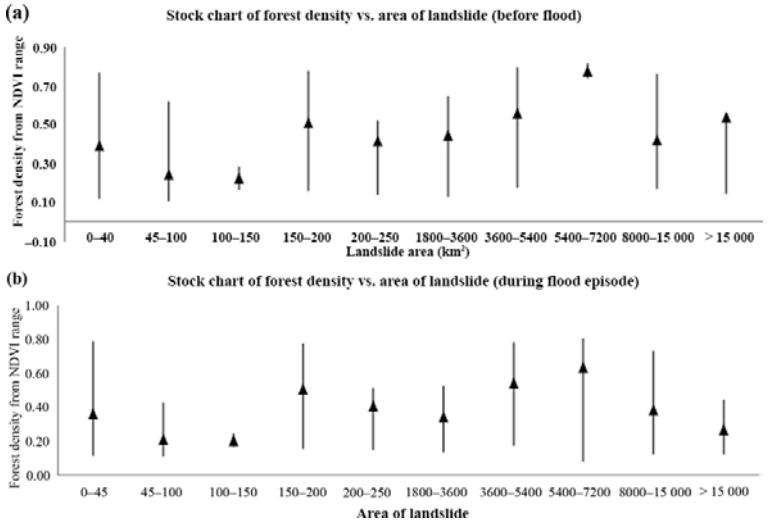

Figure 12. **(a)** Stock plot of forest density versus area of landslide before the flood. **(b)** The stock plot of forest density versus area of a landslide during flood episode.

and increases the peak of the hydrograph. Consequently, the slope of the land in the south and southwestern regions increases the speed and extent of water and sediment transportation to the Kelantan River basin during heavy monsoon rainfall. Most of the landslide-affected points were located in the topographic slope of metamorphic and quaternary rock units. However, some landslides occurred in fracture zones of weathered igneous rock units. Some large landslide-affected zones were recorded in the intersection of longitude and latitude between 5°08−02″ N, 101°58′53″ E, 5°08′14″ N, 101°59′06″ E, 5°08′24″ N, 101°59′21″ E and 5°09′03″ N, 101°59′41″ E. These landslide points were associated with N–S, NNE–SSW and NE–SW-trending fault zones. Figure 13c and d show large landslide-affected zones in the southwestern part of the Kelantan state.

Table 4. Information on statistical testing of landslide due to rainfall amount.

Regression statistics					
		Multiple R	0.0311		
		R^2	0.0010		
		Adjusted R^2	−0.0093		
		Standard error	141.4588		
		Observations	99		
ANOVA					
	Degree of freedom	Sum of squares	Mean of sum square	$F_{\text{statistic}}$	$F_{\text{significance}}$ (p value)
Regression	1	1876.59	1876.59	0.0938	0.7601
Residual	97	1 941 028.66	20 010.60		
Sum	98	1 942 905.26			

Figure 13. (a) Meander bend. **(b)** Floodplain scroll zone in the Kelantan River basin. **(c, d)** Large landslide-affected zones in the southwestern part of the Kelantan state.

5 Conclusions

Results of this investigation indicate that Landsat-8 and ALOS-2 have proven to provide successful advanced remote sensing satellite data for disaster monitoring in tropical environments. Analysis of the Landsat-8 and ALOS-2 data provided significant information for identifying high potential risk and susceptible zones for natural hazards of geological origin in the Kelantan River basin, Malaysia. Wetlands, floodplain scroll, meander bend, dendritic and sub-dendritic drainage patterns and urban areas were identified as high potential risk zones for hydrogeological hazards. Landslide recurrence regions were detected in a high-altitude segment of the south and southwestern part of the Kelantan state, which is dominated with a high density of rectangular drainage pattern and topographic slope of metamorphic and quaternary rock units. Some of the large landslide zones were associated with N–S, NNE–SSW and NE–SW-trending fault systems. Structural and topographical geology maps were produced for the Kelantan River basin that could be used to facilitate the planning of geohazards mitigation. In conclusion, the results of this investigation have great potential assistance in

terms of a total solution to flood disaster management in the Kelantan River basin by providing an important source of information to assess the potential for many natural hazards of geological origin.

Data availability. This investigation used original satellite data, which are discussed in Sect. 3.

Competing interests. The authors declare that they have no conflict of interest.

Acknowledgements. This study was conducted as a part of the Transdisciplinary Research Grant Scheme (TRGS) research project, "Detecting, mapping, and characterization of landslides and landslide assessment in Kelantan River basin during December 2014 flooding using Satellite SAR data", vote nos. R.J130000.7809.4L831 and R.J130000.7809.4L837, Ministry of Higher Education (MOHE), Malaysia. We are thankful to the Universiti Teknologi Malaysia for providing the facilities for this investigation. We also would like to express our great appreciation of Rosa Lasaponara and the anonymous reviewers for their very useful and constructive comments and suggestions for improvement of this paper.

Edited by: Rosa Lasaponara
Reviewed by: three anonymous referees

References

Abdullah, A., Nassr, S., Ghaleeb, A.: Remote sensing and geographic information system for fault segments mapping a study from Taiz area, Yemen, J. Geol. Res., 2013, 201757, https://doi.org/10.1155/2013/201757, 2013.

Akhir, J. M.: Lineament in enhanced remote sensing images: an example from the Upper Perak Valley, Perak Darul Ridwan, Geol. Soc. Malaysia Bull., 48, 115–119, 2004.

Amri, K., Mahdjoub, Y., and Guergour, L.: Use of Landsat 7 ETM+ for lithological and structural mapping of Wadi Afara Heouine area (Tahifet–Central Hoggar, Algeria), Arab. J. Geosci., 4, 1273–1287, 2011.

Arikawa, Y., Osawa, Y., Hatooka, Y., Suzuki, S., and Kankaku, Y.: Development Status of Japanese Advanced Land Observing Satellite-2, in: Vol. 7826, Proceedings of the SPIE Remote Sensing Conference, Sensors, Systems, and Next-Generation Satellites XIV, edited by: Meynart, R., Neeck, S. P., and Shimoda, H., 20–23 September 2010, Toulouse, France, https://doi.org/10.1117/12.866675, 2010.

Bannert, D.: The application of remote sensing to natural hazard of geologic orgion-experience learned from GRAS-program of Unesco and IUGS, in: Vol. XXXIII, Part B7, International Archives of Photogrammetry and Remote Sensing, Amsterdam, 2000a.

Bannert, D.: Geological application of remote sensing (GARS), an IUGS/UNESCO joint program in the new millennium, Episodes, 23, 37–39, 2000b.

Bignell, J. D. and Snelling, N. J.: Geochronology of Malayan granites, Overseas Geology and Mineral Resources, I.G.S., London, p. 72, 1977.

Blau, P.: Japan's H-IIA Rocket successfully Launches ALOS-2 Radar Satellite, Spaceflight 101, http://www.spaceflight101.com/h-iia-f24-launch-updates-alos-2.html, last access: 24 May 2014.

Carr, J. R.: Numerical analysis for the geological science, edited by: Carr, J. R., Prentice-Hall, Inc., Englewood Cliffs, New Jersey, p. 592, 1995.

Chavez, P. C. and Bauer, B.: An automatic optimum kernel-size selection technique for edge enhancement, Remote Sens. Environ., 12, 23–38, 1982.

Choi, J., Oh, H. J., Lee, H. J., Lee, C., and Lee, S.: Combining landslide susceptibility maps obtained from frequency ratio, logistic regression, and artificial neural network models using ASTER images and GIS, Eng. Geol., 124, 12–23, 2012.

Clark, C. D. and Wilson, C.: Spatial analysis of lineaments, Comput. Geosci., 20, 1237–1258, 1994.

Dai, F. C. and Lee, C. F.: Landslide characteristics and slope instability modeling using GIS, Lantau Island, Hong Kong, Geomorphology, 42, 213–228, 2002.

Department of Minerals and Geoscience Malaysia: Quarry Resource Planning for the State of Kelantan, Osborne and Chappel Sdn. Bhd., Kuala Lumpur, Malaysia, 2003.

Eagleman, J. R. and Lin, W. C.: Remote Sensing of Soil Moisture by a 21-cm Passive Radiometer, J. Geophys. Res., 81, 3660–3666, 1976.

Eckardt, R., Berger, C., Thiel, C., and Schmullius, C.: Removal of Optically Thick Clouds from Multi-Spectral Satellite Images Using Multi-Frequency SAR Data, Remote Sensing, 5, 2973–3006, https://doi.org/10.3390/rs5062973, 2013.

Eliason, E. M. and McEwen, A. S.: Adaptive Box Filters for Removal of Random Noise from Digital Images, Photogramm. Eng. Remote Sens., 56, 453–458, 1990.

ERSDAC – Earth Remote Sensing Data Analysis Center: PALSAR user's guide, 1st Edn., Japan Space SystemsEarth Remote Sensing Division, Japan, March 2006.

Franceschetti, G. and Lanari, R.: Synthetic aperture radar processing, CRC Press, Boca Raton, 1999.

Gelautz, M., Frick, H., Raggam, J., Burgstaller, J., and Leberl, F.: SAR image simulation and analysis of alpine terrain, ISPRS J. Photogramm. Remote Sens., 53, 17–38, 1998.

Ghani, A. A.: Plutonism, in: Geology of Peninsular Malaysia, edited by: Hutchison, C. S. and Tan, D. N. K., Geological Society of Malaysia, Kuala Lumpur, 211–232, 2009.

Guzzetti, F., Carrara, A., Cardinali, M., and Reichenbach, P.: Landslide hazard evaluation: a review of current techniques and their application in multi-scale study, Central Italy, Geomorphology, 31, 181–216, 1999.

Hamimi, Z., El-Sawy, E. S. K., El-Fakharani, A., Matsah, M., Shujoon, A., and El-Shafei, M. K.: Neoproterozoic structural evolution of NE-trending Ad-Damm Shear Zone, Arabian Shield, Saudi Arabia, J. Asian Earth Sci., 99, 51–63, 2014.

Haralick, R. M., Sternberg, S. R., and Zhuang, X.: Image Analysis Using Mathematical Morphology, IEEE T. Pattern Anal. Mach. Intel., PAMI-9, 532–550, 1987.

Harris, J. F., Tailor, G. L., and Walper, J. L.: Relation of deformational fractures in sedimentary rocks to regional and local structure, Am. Assoc. Petrol. Geol. Bull., 44, 1853–1873, 1960.

Harun, Z.: Late Mesozoic-Early Tertiary faults of Peninsular Malaysia, in: Geological Society of Malaysia Annual Geological Conference, 26–27 May 2002, Kota Bharu, Kelantan, Malaysia, 2002.

Hashim, M., Ahmad, S., Johari, M. A. M., and Pour, A. B.: Automatic lineament extraction in a heavily vegetated region using Landsat Enhanced Thematic Mapper (ETM+) imagery, Adv. Space Res., 51, 874–890, 2013.

Henderson, F. M. and Lewis, A. J.: Principles and applications of imaging radar, manual of remote sensing, in: Vol. 2, 3rd Edn., John Wiley and Sons, New York, 886 pp., 1998.

Heng, G. S., Hoe, T. G., and Hassan, W. F. W.: Gold mineralization and zonation in the state of Kelantan, Geol. Soc. Malaysia Bull., 52, 129–135, 2006.

Igarashi, T.: ALOS Mission requirement and sensor specifications, Adv. Space Res., 28, 127–131, 2001.

Irons, J. R., Dwyer, J. L., and Barsi, J. A.: The next Landsat satellite: The Landsat Data Continuity Mission, Remote Sens. Environ., 145, 154–172, 2012.

Jackson, T. J. and Schmugge, T. J.: Passive Microwave Remote Sensing System for Soil Moisture: Some Supporting Research, IEEE T. Geosci. Remote, 27, 225–235, 1989.

Japan Aerospace Exploration Agency: ALOS-2/PALSAR-2 Level 1.1/1.5/2.1/3.1 GeoTIFF Product Format Description, http://www.eorc.jaxa.jp/ALOS-2/en/doc/format.htm (last access: 22 December 2015), 2014.

Jensen, J. R.: Introductory Digital Image Processing: A remote sensing perspective, 3rd Edn., Pearson Prentice Hall, Upper Saddle River, NJ, 276–287, 2005.

Ju, J. and Roy, D. P.: The availability of cloud-free Landsat ETM+ data over the conterminous United States and globally, Remote Sens. Environ., 112, 1196–1211, 2008.

Kankaku, Y., Osawa, Y., Hatooka, Y., and Suzuki, S.: Overview of Advanced Land Observing Satellite-2 (ALOS-2), in: Proceedings of ISPRS Technical Commission VIII Symposium, 9–12 August 2010, Kyoto, Japan, 2010.

Komac, M.: A landslide susceptibility model using the Analytical Hierarchy Process method and multivariate statistics in perialpine Slovenia, Geomorphology, 74, 17–26, 2006.

Lacava, T., Greco, M., and Leo, E.: Monitoring soil wetness variations by means of satellite passive microwave observations: the hydroptimet study case, Nat. Hazards Earth Syst. Sci., 5, 583–592, 2005.

Lee, J. S. and Jurkevich, I.: Speckle filtering of synthetic aperture radar images: a review, Remote Sens. Rev., 8, 313–340, 1994.

Malczewski, J.: GIS and Multi-criteria Decision Analysis, John Wiley and Sons, New York, 1999.

Mardiana, S., Ahmad, A., and Osman, K.: Capability of RADARSAT data in monsoon flood monitoring, GIS Development, 1–6, http://a-a-r-s.org/aars/proceeding/ACRS2000/Papers/ENV00-10.htm (last access: July 2017), 2000.

Melgani, F.: Contextual reconstruction of cloud contaminated multitemporal multispectral images, IEEE T. Geosci. Remote, 44, 442–455, 2006.

Metcalfe, I.: The Bentong-Raub Suture Zone, J. Asian Earth Sci., 18, 691–712, 2000.

Metcalfe, I.: Tectonic evolution of the Malay Peninsula, J. Asian Earth Sci., 76, 195–213, 2013a.

Metcalfe, I.: Gondwana dispersion and Asian accretion: Tectonic and palaeogeographic evolution of eastern Tethys, J. Asian Earth Sci., 66, 1–33, 2013b.

Morelli, M. and Piana, F.: Comparison between remote sensed lineaments and geological structure in intensively cultivated hills (Monferrato and Langhe domains, NW Italy), Int. J. Remote Sens., 27, 4471–4493, 2006.

Nazaruddin, D. A., Fadilah, N. S. M., Zulkharnain, Z., Omar, S. A. S., and Ibrahim, M. K. M.: Geological Studies to Support the Tourism Site: A Case Study in the *Rafflesia* Trail, Near Kampung Jedip, Lojing Highlands, Kelantan, Malaysia, Int. J. Geosci., 5, 835–851, 2014.

Plank, S., Twele, A., and Martinis, S.: Landslide mapping in vegetated areas using change detection based on optical and polarimetric SAR data, Remote Sensing, 8, 307, https://doi.org/10.3390/rs8040307, 2016.

Pour, B. A. and Hashim, M.: Structural geology mapping using PALSAR data in the Bau gold mining district, Sarawak, Malaysia, Adv. Space Res., 54, 644–654, 2014.

Pour, B. A. and Hashim, M.: Structural mapping using PALSAR data in the Central Gold Belt Peninsular Malaysia, Ore Geol. Rev., 64, 13–22, 2015a.

Pour, B. A. and Hashim, M.: Integrating PALSAR and ASTER data for mineral deposits exploration in tropical environments: a case study from Central Belt, Peninsular Malaysia, Int. J. Image Data Fusion, 6, 170–188, 2015b.

Pour, B. A., Hashim, M., and van Genderen, J.: Detection of hydrothermal alteration zones in a tropical region using satellite remote sensing data: Bau gold field, Sarawak, Malaysia, Ore Geol. Rev., 54, 181–196, 2013.

Pour, B. A., Hashim, M., and Marghany, M.: Exploration of gold mineralization in a tropical region using Earth Observing-1 (EO1) and JERS-1 SAR data: a case study from Bau gold field, Sarawak, Malaysia, Arab. J. Geosci., 7, 2393–2406, 2014.

Pradhan, B.: Flood susceptible mapping and risk area delineation using logistic regression, GIS and remote sensing, J. Spat. Hydrol., 9, 2009.

Pradhan, B. and Youssef, A. M.: A 100-year maximum flood susceptibility mapping using integrated hydrological and hydrodynamic models: Kelantan River Corridor, Malaysia, J. Flood Risk Manage., 4, 189–202, https://doi.org/10.1111/j.1753-318X.2011.01103.x, 2011.

Pradhan, B., Shafiee, M., and Pirasteh, S.: Maximum flood prone area mapping using RADARSAT images and GIS: Kelantan river basin, Int. J. Geoinform., 5, 11–23, 2009.

Raharimahefa, T. and Kusky, T. M.: Stuctural and remote sensing studies of the southern Betsimisaraka Suture, Madagascar, Gondwana Res., 10, 186–197, 2007.

Raharimahefa, T. and Kusky, T. M.: Structural and remote sensing analysis of the Betsimisaraka Suture in northeastern Madagascar, Gondwana Res., 15, 14–27, 2009.

Rahman, C. A. and Mohamed, K. R.: Pemetaan Awalan Sumber Warisan Geologi Negeri Kelantan, in: Geological Heritage of Malaysia (Geoheritage Mapping and Geosite Characterization), edited by: Komoo, I., Tjia, H. D., and Leman, M. S., LESTARI UMK, Bangi, 2001.

Raj, J. K.: Geomorphology, in: Geology of Peninsular Malaysia, edited by: Hutchison, C. S. and Tan, D. N. K., Geological Society of Malaysia, Kuala Lumpur, 5–29, 2009.

Ramli, M. F., Tripathi, N. K., Yusof, N., Shafri, H. Z. M., and Rahman, Z. A.: Lineament mapping in a tropical environment using Landsat imagery, Int. J. Remote Sens., 30, 6277–6300, 2009.

Razak, K. A., Santangelo, M., Van Westen, C. J., Straatsma, M. W., and de Jong, S. M.: Generating an optimal DTM from airborne laser scanning data for landslide mapping in a tropical forest environment, Geomorphology, 190, 112–125, 2013.

Research Systems, Inc.: ENVI Tutorials, Research Systems, Inc., Boulder, CO, 2009.

Richard, J. A. and Jia, X.: Remote Sensing Digital Image Analysis, Springer-Verlag, New York, p. 363, 1999.

Richter, B., Schmidtke, E., Fuller, M., Harbury, N., and Samsudin, A. R.: Palaeomagnetism of Peninsular Malaysia, J. Asian Earth Sci., 17, 477–519, 1999.

Robinson, C., Kusky, T., El-Baz, F., and El-Etr, H.: Using Radar Data to Assess Structural Controls from Variable Channel Morphology: Examples from the Eastern Sahara, in: Proceeding of the Thirteen International Conference on Applied Geologic Remote Sensing, 1–3 March 1999, Vancouver, Canada, 1999.

Rosenqvist, A., Shimada, M., and Chapman, B.: An overview of the JERS-1 SAR Global Boreal Forest Mapping (GBFM) project, in: Vol. 2, Proceedings of Geoscience and Remote Sensing Symposium, IGARRS 0.4, 20–24 September 2004, Anchorage, AK, USA, 1033–1036, 2004.

Roy, D. P., Wulder, M. A., Loveland, T. A., et al.: Landsat-8: Science and product vision for terrestrial global change research, Remote Sens. Environ., 145, 154–172, 2014.

Russ, J. C.: The Image Processing Handbook, CRC Press, Boca Raton, FL, p. 744, 2002.

Saaty, T. L.: The Analytical Hierarchy Process, McGraw Hill, New York, 1980.

Saaty, T. L. and Vargas, G. L.: Prediction, Projection and Forecasting, Kluwer Academic Publishers, Dordrecht, 1991.

Saaty, T. L. and Vargas, G. L.: Models, Methods, Concepts, and Applications of the Analytic Hierarchy Process, Kluwer Academic Publisher, Boston, 2001.

Sabins, F. F.: Remote sensing: Principal and Interpretation, 3rd Edn., W. H. Freeman and Co., Long Grove, Illinois, USA, 1996.

Schowengerdt, R. A.: Remote sensing: models and methods for image processing, 3rd Edn., Academic Press, Elsevier, Burlington, MA, 229–243, 2007.

Schwartz, M. O., Rajah, S. S., Askury, A. K., Putthapiban, P., and Djaswadi, S.: The Southeast Asian Tin Belt, Earth Sci. Rev., 38, 95–293, 1995.

Shahabi, H. and Hashim, M.: Landslide susceptibility mapping using GIS-based statistical models and remote sensing data in tropical environment, Scient. Rep., 5, 9899, https://doi.org/10.1038/srep09899, 2015.

Sheng, Y. and Xia, Z. G.: A comprehensive evaluation of filters for radar speckle suppression, in: Vol. 3, Remote sensing for sustainable future, Geoscience and Remote Sensing Symposium, IGARSS.96, Lincoln, NE, USA, 1559–1561, 1996.

Shimada, M.: ALOS-2 science program, in: Proceedings of IGARSS (IEEE international Geoscience and Remote Sensing symposium), 21–26 July 2013, Melbourne, Australia, 2013.

Shimada, M. and Isoguchi, O.: JERS-1 SAR mosaics of SouthEastAsia using calibrated path images, Int. J. Remote Sens., 23, 1507–1526, 2002.

Shimada, M., Watanabe, M., Motooka, T., Kankaku, Y., and Suzuki, S.: Calibration and validation of the PALSAR-2, in: Proceedings of the IGARSS (International Geoscience and Remote Sensing Symposium) 2015, 26–31 July 2015, Milan, Italy, 2015.

Summerfield, M. A: Global Geomorphology. An Introduction to the Study of Landforms, in: Part IV, chap. 16, John Wiley Inc., Longman, New York, 405–430, 1991.

Suzen, M. L. and Doyuran, V.: Data driven bivariate landslide susceptibility assessment using geographical information systems: a method and application to Asarsuyu catchment, Turkey, Eng. Geol., 71, 303–321, 2004.

Suzen, M. L. and Toprak, V.: Filtering of satellite images in geological lineament anlyses: an application to a fault zone in Central Turkey, Int. J. Remote Sens., 19, 1101–1114, 1998.

Suzuki, S.: Advanced Land Observing Satellite-2 "DAICHI-2" (ALOS-2) – Mission talk by team leaders, JAXA, http://global.jaxa.jp/projects/sat/alos2/leaders.html, last access: May 2014.

Suzuki, S., Kankaku, Y., Imai, H., and Osawa, Y.: Overview of ALOS-2 and ALOS-3, in: Vol. 8528, Proceedings of SPIE, Earth Observing Missions and Sensors: Development, Implementation, and Characterization II, 29 October 2012, Kyoto, Japan, https://doi.org/10.1117/12.979184, 2012.

Sveinsson, J. R. and Benediktsson, J. A.: Speckle reduction and enhancement of SAR image in the wavelet domain, in: Vol. 1, Remote sensing for sustainable future, Geoscience and Remote Sensing Symposium, IGARSS.96, Lincoln, NE, USA, 63–66, 1996.

Tan, B. K.: "Suture Zone" in peninsular Malaysia and Thailand: Implications for paleotectonic reconstruction of Southeast Asia, J. S. Asian Earth Sci., 13, 243–249, 1996.

Tehrany, M. S., Pradhan, B., and Jebur, M. N.: Spatial prediction of flood susceptible areas using rule based decision tree (DT) and a novel ensemble bivariate and multivariate statistical models in GIS, J. Hydrol., 504, 69–79, 2013.

Thome, K., Palluconi, F., Takashima, T., and Masuda, K.: Atmospheric Correction of ASTER, IEEE T. Geosci. Remote, 36, 1119–1211, 1998.

Thurmond, A. K., Abdelsalam, M. G., and Thurmond, J. B.: Optical-radar-DEM remote sensing data integration for geological mapping in the Afar Depression, Ethiopia, J. Afr. Earth Sci., 44, 119–134, 2006.

Tjia, H. D.: Major faults of Peninsular Malaysia on remotely sensed images, Sains Malaysiana, 18, 101–114, 1989.

Tjia, H. D. and Harun, Z.: Regional structures of Peninsular Malaysia, Sains Malaysiana, 14, 95–107, 1985.

Tripathi, N. K. and Gokhale, V. G. K.: Directional morphological image transforms for lineament extraction from remotely sensed images, Int. J. Remote Sens., 21, 3281–3292, 2000.

Unjah, T., Komoo, I., and Mohamad, H.: Pengenalpastian Sumber Warisan Geologi di Negeri Kelantan, in: Geological Heritage of Malaysia (Geoheritage Mapping and Geosite Characterization), edited by: Komoo, I., Tjia, H. D., and Leman, M. S., LESTARI UMK, Bangi, 2001.

van der Pluijm, B. A. and Marshak, S.: Earth Structure – An Introduction to Structural Geology and Tectonics, WCB–McGraw–Hill, New York, 1997.

Vincent, R.K., 1997. Fundamentals of Geological and Environmental Remote Sensing, Prentice Hall, New Jersey, pp: 366.

Woodhouse, I. H.: Introduction to microwave remote sensing, CRC Press, Taylor & Francis Group, Boca Raton, 2006.

Yalcin, A.: GIS-based landslide susceptibility mapping using analytical hierarchy process and bivariate statistics in Ardesen (Turkey): Comparisons of results and confirmations, Catena, 72, 1–12, 2008.

Yalcin, A., Reis, S., Aydinoglu, A. C., and Yomralioglu, T.: A GIS-based comparative study of frequency ratio, analytical hierarchy process, bivariate statistics and logistics regression methods for landslide susceptibility mapping in Trabzon, NE Turkey, Catena, 85, 274–287, 2011.

Yamamoto, T., Kawano, I., Iwata, T., Arikawa, Y., Itoh, H., Yamamoto, M., and Nakajima, K.: Autonomous Precision Orbit Control of ALOS-2 for Repeat-Pass SAR Interferometry, in: Proceedings of IGARSS (IEEE International Geoscience and Remote Sensing Symposium), 21–26 July 2013, Melbourne, Australia, 2013.